Title

BMPR1A maintains skeletal stem cell properties in craniofacial development and craniosynostosis.

Journal

Science Translational Medicine, 13(583)

Authors

Maruyama, Takamitsu

Stevens, Ronay

Boka, Alan

et al.

Publication Date

2021-03-03

DOI

10.1126/scitranslmed.abb4416

Peer reviewed

HHS Public Access

Author manuscript

Sci Transl Med. Author manuscript; available in PMC 2021 November 13.

Published in final edited form as:

Sci Transl Med. 2021 March 03; 13(583): . doi:10.1126/scitranslmed.abb4416.

BMPR1A maintains skeletal stem cell stemness in craniofacial development and craniosynostosis

Takamitsu Maruyama[1,3], **Ronay Stevens**[1], **Alan Boka**[1], **Laura DiRienzo**[1], **Connie Chang**[1], **H-M Ivy Yu**[1], **Katsuhiko Nishimori**[6], **Clinton Morrison**[4], **Wei Hsu**[1,2,5,*]

[1]Center for Oral Biology, University of Rochester Medical Center, Rochester, NY 14642, USA

[2]Department of Biomedical Genetics, University of Rochester Medical Center, Rochester, NY 14642, USA

[3]Department of Dentistry, University of Rochester Medical Center, Rochester, NY 14642, USA

[4]Department of Surgery, University of Rochester Medical Center, Rochester, NY 14642, USA

[5]Stem Cell and Regenerative Medicine Institute, University of Rochester Medical Center, Rochester, NY 14642, USA

[6]Department of Bioregulation and Pharmacological Medicine and Department of Obesity and Internal Inflammation, Fukushima Medical University, Fukushima City, Japan

Abstract

Skeletal stem cells identified and isolated from the suture mesenchyme exhibit long-term self-renewal, clonal expansion, and multipotency. These suture stem cells (SuSCs) residing in the suture midline are the skeletal stem cell population responsible for calvarial development, homeostasis, injury repair, and regeneration. The high engraftment of SuSCs and their ability to replace the damaged skeleton support their potential uses for stem cell-based therapy. Here we identify Bmpr1a as a regulator essential for SuSC self-renewal and SuSC-mediated bone formation. SuSC-specific disruption of Bmpr1a causes precocious differentiation, leading to craniosynostosis initiated in the suture midline – stem cell niche. Human SuSCs are also characterized using BMPR1A as a cell surface marker. An ex vivo system further demonstrates the maintenance of SuSC stemness in an extended period without losing the osteogenic ability. This study significantly advances our knowledge base of congenital deformity and regenerative medicine mediated by skeletal stem cells.

One-sentence Summary:

Stemness of skeletal stem cells in the calvarium is maintained by Bmpr1a whose disruption causes stem cell depletion and suture synostosis.

*Corresponding Author: Phone 585-275-7802, FAX 585-276-0190, Wei_Hsu@urmc.rochester.edu.

Author contributions

T.M., K.N, and W.H. conceived and designed the experiments. T.M. and W.H. wrote the paper. T.M., R.S., L.D., C.C., H.I.Y., C.M., and W.H. performed the experiments and analyzed the data.

Keywords

Calvarial morphogenesis; Cranial suture; Skeletal stem cell; Congenital disorder; Axin2; Wnt; BMP

Introduction

Large craniofacial bone defects caused by various conditions, including trauma, infection, tumors, congenital disorders, and progressive deforming diseases, are major health issues (1). The autologous bone graft is a recommended procedure for such extensive skeletal repairs but their success remains highly challenging owing to several limitations (1, 2), leading to the exploration of alternative approaches (3, 4). Stem cell-based therapy is particularly attractive and promising given to recent advancements in the characterization of skeletal stem cells in craniofacial and body skeletons (5–11). Craniofacial bone is mainly formed through intramembranous ossification, a process different from the endochondral ossification required for the body skeleton (12). Because of distinct stem cell properties (5, 13), it is necessary to study skeletal stem cells, e.g. suture stem cells (SuSCs), naturally programmed to form intramembranous bones during craniofacial skeletogenesis (5). The lack of a cell surface marker for stem cell isolation and the missing of a method to maintain the stemness ex vivo are two critical hurdles, restricting further advances for the field of skeletal regeneration.

Craniosynostosis, affecting one in ~2,500 individuals, is one of the most common congenital deformities and is caused by premature suture closure (14). The suture serving as the growth center for calvarial morphogenesis is the equivalent of the growth plate in the long bone. Excessive intramembranous ossification caused by genetic mutation has been well-established to promote suture fusion (15), including the loss of Axin2 causing craniosynostosis in mice and humans (16, 17). In 2010, our genetic analyses further revealed that craniosynostosis can be caused by mesenchymal cell fate switching, leading to suture closure via endochondral ossification (18). The Axin2-mediated Wnt signaling regulates the interplay of Bone Morphogenetic Protein (BMP) and fibroblast growth factor (FGF) pathways critical for skeletal lineage commitment, supporting the existence of skeletal stem cells within the suture mesenchyme (18). Because of Axin2 expression in the presumptive niche site tightly linked to suture patency, we were able to identify Axin2 expressing SuSCs essential for calvarial development, homeostasis, and injury-induced repair (5). The Axin2+ SuSCs qualified for the modern and more rigorous stem cell definition in which they exhibit not only long-term self-renewal, clonal expansion, differentiation, and multipotency but also the ability to repair skeletal defects by direct engraftment and replacement of damaged tissue. However, the mechanism underlying the regulation of SuSC properties and the causal link of SuSC dysregulation to congenital birth defects remain highly elusive.

Results

Identification of BMP pathway in Axin2-expressing SuSCs

Our isolation of SuSCs prompted us to examine their gene expression profile for identifying stem cell regulators. Using the *Axin2*^{GFP} mouse model (Fig. S1A), we isolated the Axin2-expressing cell population with high expression of GFP (Axin2^{+}/GFP^{hi}) and non-expressing cell population negative for GFP (Axin2^{-}/GFP^{-}) from the P28 *Axin2*^{GFP} suture mesenchyme. Microarray analysis comparing SuSCs (Axin2+) and non-SuSCs (Axin2-) revealed approximately 9,000 genes with significant differences (p-value < 0.05, n=3), followed by pathway analysis using Ingenuity pathway (IPA) software (Ingenuity® Systems). We obtained two scores: an enrichment score, statistically evaluating the accumulation of gene set in each pathway, and a Z-score assessing the activation state of the signal by the match of observed and predicted up/down-regulation patterns (19). In SuSCs, most of the identified signaling pathways were inactive but the BMP pathway exhibited significant activation (Fig. S2A, p-value < 10^{-13}, z-score > 2.3). The heatmap further showed that seven BMP ligands and one type I receptor (Bmpr1a) are upregulated while two negative regulators (Smad7 and Smurf1) downregulated in SuSCs (Fig. S2B). The results suggested that BMP ligands signal through Bmpr1a type I receptor to activate the pathway. Therefore, we examined Bmpr1a expression in the *Axin2*^{lacZ} model in which SuSCs are marked by lacZ. Double labeling of Axin2 and Bmpr1a identified Axin2+ SuSCs expressing Bmpr1a at P28 (Fig. S2C–E), implying a role of BMP-Bmpr1a signaling in the SuSC regulation.

The requirement of Bmpr1a for SuSC-mediated calvarial development and homeostasis

To further delineate the functional importance of BMP signaling in SuSCs, we studied its type I receptors in calvarial morphogenesis (20, 21). There are three type I receptors, Bmpr1a, Bmpr1b, and Acvr1, identified in BMP signal transduction (20, 21). It is more feasible to accomplish their examinations in comparison to a large family of BMP ligands. Mice with global inactivation of *Bmpr1b* is viable while the null mutation of Bmpr1a or Acvr1 is associated with embryonic lethality due to defective mesodermal formation (22–25). Therefore, we developed *Bmpr1a*^{Ax2} *(Axin2*$^{Cre\text{-}Dox}$*; Bmpr1aFx/Fx)* and *Acvr1*^{Ax2} *(Axin2*$^{Cre\text{-}Dox}$*; Acvr1Fx/Fx)* models, permitting doxycycline (Dox)-inducible deletion of Bmpr1a and Acvr1 in the Axin2+ SuSCs, respectively. For the calvarial formation study, Dox was administrated from embryonic day (E) 16.5 to P3 for Cre-dependent gene deletion (Fig. 1A). The efficiency of Cre-mediated recombination in Axin2+ SuSCs and their derivatives was demonstrated by using an R26RlacZ reporter strain (Fig. S3A, B). The *Bmpr1a*^{Ax2}, but not *Bmpr1b* and *Acvr1*^{Ax2}, mice displayed craniofacial anomalies at 2 months (Fig. 1B, E, H, and Fig. S4A–B). We could easily identify *Bmpr1a*^{Ax2} mutants due to abnormal skull shape. Micro-computed tomography (μCT) analysis and histology further revealed calvarial bone and suture closure abnormalities caused by the loss of Bmpr1a (Fig. 1C–D, F-G, I-J, K-N, and Fig. S4). The *Bmpr1a*^{Ax2} skull exhibited a dome shape and was significantly shorter during neonatal development (Fig. S4A, C, E–F, p-value < 0.05). Alizarin red staining and histology (Fig. S5), and μCT analyses (Fig. S6) identified multiple synostoses in the internasal, anterior frontal, sagittal, lambdoid, and squamosal sutures of *Bmpr1a*^{Ax2}. Immunostaining shows not only the efficacy of Bmpr1a ablation in the mutant

but also the specificity of the Bmpr1a antibody (Fig. S3C, D). The results indicate a specific requirement of Bmpr1a in SuSCs during calvarial morphogenesis.

We previously demonstrated that Axin2-expressing cells function as skeletal stem cells in calvarial development and homeostasis (5). To test if Bmpr1a regulates adult SuSCs, we induced its deletion in the fully mature skull. In humans, the growth of the skull reaches 90% of adult size in the first year, and 95% of adult size by 6 years of age (26). The skull size in teenagers is identical to that of adults. In mice, acute development of the skull is completed with SuSCs highly restricted to the suture midline at P28 (5). Therefore, we administrated Dox to the P28 *Bmpr1a*^{Ax2} mice for 7 days (Fig. 1O). Three months after the Dox treatment, the mutants were examined by μCT and histology. The deletion of Bmpr1a in adult SuSCs resulted in aberrant suture morphogenesis and multiple sutural synostoses (Fig. 1P–U), suggesting an essential role of Bmpr1a in SuSC-mediated calvarial development and homeostasis.

Craniosynostosis is initiated in the midline of the Bmpr1a^{Ax2} suture

A time-course study was performed to decipher the suture closure process. Dox-inducible deletion of Bmpr1a was conducted from E15.5-P3, followed by alizarin red and Goldner's trichrome staining analyses at P0, P7, and P14 (Fig. 2). At P0, the Bmpr1a deletion caused a wider suture (Fig. 2A, D, and G–H). However, abnormal ossification arising within the suture mesenchyme was evident at P7 and P14 (Fig. 2B–C, E–F, I–L), ultimately leading to suture closure (Fig. 1D, L). This finding suggested an extremely interesting mechanism in which aberrant ossification is initiated in the suture midline and moves toward the osteogenic fronts.

Calvarial bones are formed through osteoblast-mediated intramembranous ossification. To delineate the aberrant ossification process caused by the SuSC-specific deletion of Bmpr1a, we examined osteoblast proliferation and differentiation. Immunostaining of Ki67, a marker for cells undergoing mitotic divisions, revealed that cell proliferation is mostly quiescent in the suture mesenchyme but active at the osteogenic fronts where intramembranous ossification occurs towards the suture midline (Fig. 3A, C). However, the number of Ki67+ cells was not only increased at the osteogenic fronts but aberrantly elevated in the suture mesenchyme (Fig. 3B, D). Next, we examined osteoprogenitor and osteoblast cells by immunostaining of Osterix (Osx) and in situ hybridization of type I collagen (Col1), respectively. At P0, Osx+ osteoprogenitors were detected only at the osteogenic fronts of control and *Bmpr1a*^{Ax2} (Fig. 3E–F). However, at P3, we detected a severe elevation of Osx+ osteoprogenitors in the suture mesenchyme caused by the Bmpr1a deletion in SuSCs (Fig. 3G–J). Similar drastic increases in Col1+ osteoblasts were found in the *Bmpr1a*^{Ax2} calvaria (Fig. 3K–L). No type II collagen (Col2) positive chondrocyte was detected in the mutant (Fig. S3E–G), suggesting that the loss of Bmpr1a does not promote stem cell fate change and the aberrant suture closure was not caused by ectopic chondrogenesis and endochondral ossification. Our findings strongly support aberrant ossification is initiated in the suture mesenchyme rather than the osteogenic fronts. To our knowledge, this type of process to mediate suture closure has never been reported for craniosynostosis. Typically, excessive ossification is initiated at the osteogenic fronts and then moves toward the midline

to cause suture synostosis. The study of the *Bmpr1a*^{Ax2} model had led us to uncover a new pathogenic mechanism for craniosynostosis and provided a unique opportunity to further our understanding of the regulation and importance of SuSCs in suture patency. It is possible that Bmpr1a is required for the maintenance of SuSCs and their depletion result in aberrant suture closure.

Signaling effects of Bmpr1a on SuSCs in developing suture

To examine the downstream pathways affected by the loss of Bmpr1a in SuSCs, we first analyzed canonical BMP signaling mediated by Smad proteins. Immunostaining showed comparable expression of phosphorylated Smad1/5/8 in the osteogenic front and periosteum of control and *Bmpr1a*^{Ax2} (Fig. S7A–B). However, slightly but noticeably reduced expression was found in the *Bmpr1a*^{Ax2} suture midline (Fig. S7C–D). We also investigated if the noncanonical effects of Bmpr1a are altered by the mutation. Noncanonical BMP signaling is known to be mediated through downstream effectors, e.g. Tak1, JNK, and p38 kinases (27). The staining of phosphorylated TAK1 indicated its strong expression mainly in the osteogenic front (Fig. S7E). The amount of phosphorylated TAK1 was also comparable in the osteogenic front and suture region of control and *Bmpr1a*^{Ax2} (Fig. S7E–F). The examination of Tak1 downstream mitogen-activated protein (MAP) kinases showed strong activation of p38, but not JNK (Fig. S7G–J). The other MAP kinase Erk was also highly stimulated in the mutant (Fig. S7K–L). The involvement of p38 and Erk in Bmpr1a-mediated regulation of SuSCs during suture morphogenesis agreed with previous notions that P38 and Erk are critical for suture morphogenesis (28–30). However, a noncanonical pathway independent of Tak1 likely mediates Bmpr1a downstream effects. The deletion of Bmpr1a reduced canonical but enhanced noncanonical signaling cascade in SuSCs, leading to precocious differentiation in the suture midline and craniosynostosis.

Bmpr1a is required for maintenance of SuSCs

Cell proliferation and osteoprogenitor/osteoblast numbers greatly enhanced in the *Bmpr1a*^{Ax2} suture mesenchyme (Fig. 3) implied a potential role of Bmpr1a in stem cell maintenance. The loss of Bmpr1a might deplete the stem cell population leading to precocious osteoblast differentiation and intramembranous ossification. To test our hypothesis, we examined SuSC characteristics of *Bmpr1a*^{Ax2}. Using an in vivo clonal expansion analysis, we previously showed the ability of a single Axin2+ SuSC to generate calvarial bone upon implantation into the kidney capsule (5). With limiting dilution analysis, we further established a quantitative method to examine stem cell clonal expansion in the transplanted kidney thereby measuring stem cell frequency (5). Therefore, we investigated if Bmpr1a deficiency affects the clonal expansion and number of SuSCs. First, various amounts of cells isolated from the control and *Bmpr1a*^{Ax2} sutures were implanted into the kidney capsule, followed by von Kossa staining and histological evaluation (Fig. 4A–L). Transplantation of 10^3-10^5 control cells had a 100% success rate on bone formation (Fig. 4M). At 10^2 cells, it's still possible to detect ectopic bones (Fig. 4M). In contrast, we couldn't detect ectopic bone formation by transplantation of 10^2-10^3 *Bmpr1a*^{Ax2} cells (Fig. 4M). The success rate was 100% at 10^5 cells but decreased at 10^4 cells for the mutant (Fig. 4M). Estimating stem cell frequency using ELDA software, we found the loss of Bmpr1a significantly decreases SuSC frequency in the P5 suture (Fig. 4M; control: 1 in 216 cells

and *Bmpr1a*^{Ax2}: 1 in 23572 cells, p-value = 5.7×10^{-6}). Furthermore, immunostaining analysis revealed a significant loss of Axin2+ SuSCs in the *Bmpr1a*^{Ax2} suture (Fig. 4N–P; control – 4.9 ± 0.3%, *Bmpr1a*^{Ax2} – 0.6 ± 0.2%, p-value < 0.01, n=3, mean ± SEM, student t-test). These data suggested that Bmpr1a plays an essential role in SuSC stemness and maintenance. The loss of Bmpr1a in SuSCs induces their precocious differentiation and aberrant ossification in the suture midline, leading to craniosynostosis.

Preservation of SuSC stemness in culture

The bone formation analysis with kidney capsule transplantation can faithfully assess SuSC properties in vivo but it is extremely important to develop a protocol capable of maintaining their stemness in vitro. Conventional culture methods for mesenchymal stromal cells (MSCs) unfortunately are unable to preserve SuSC stemness. The sphere culture has been shown to maintain the properties of neural and mammary stem cells, recapitulating the in vivo characteristics. After labor-intensive efforts, we established a cultural protocol for cells isolated from the suture mesenchyme (Fig. S8A). First, the isolated suture cells grew into primary (1^0) spheres in single-cell suspension culture with very low seeding density. Next, 1^0 spheres were dissociated into single cells and able to form secondary (2^0) spheres (Fig. S8B–D). In each passage, 10^4 cells were seeded at the beginning of the sphere culture. After serial re-plating, suture spheres continued to form without notable decreases in number, implying the presence of SuSCs with self-renewing ability. We were able to show SuSC self-renewal by culturing the spheres up to 5 passages (Fig. S8E). The average sphere size remained comparable in different passages (Fig. S8L). The time-course study suggested a sphere formed by the growth of a single cell (Fig. S8F–K). To determine the cellular origin, we performed tracing of Axin2+ cells using the *Axin2*$^{Cre\text{-}Dox}$*; R26RTomato* model (Fig. S1B). Suture cells isolated from the *Axin2*$^{Cre\text{-}Dox}$*; R26RTomato* mice with Dox treatment for 3 days were cultured in the absence of Dox. Only a very small portion of cells was positive for Tomato at the beginning of the single-cell suspension culture (Fig. 5A–C, 5 ± 0.3%, n = 3, mean ± SEM). After 2 weeks, a majority of the spheres consisted of all Tomato+ cells, suggesting they derived from a single Axin2+ cell with clonal expansion ability (Fig. 5D–H, 88 ± 2.2%, n = 3, mean ± SEM). We didn't detect chimeric spheres (a mixture of Tomato+ and Tomato– cells), indicating that suture spheres are not formed by aggregation, a common concern for this culture approach. The multipotency test showed that 3^0 spheres can develop into osteoblast cells to form mineralized nodules, and into chondrogenic cells upon ex vivo differentiation (Fig. S8M–O).

To examine the clonal expansion and bone-forming abilities of suture spheres in vivo, we performed kidney capsule transplantation analysis. We implanted 30 spheres, which are formed using cells isolated from the *Axin2*$^{Cre\text{-}Dox}$*; R26RTomato* suture, into the kidney capsule. The results demonstrated successful expansion, colonization, and engraftment from the in vitro cultured Axin2-expressing cells (Fig. 5I–K). The transplanted 1^0 spheres or 3^0 spheres were able to generate bones resembling calvarial bones (Fig. 5L–N; Fig. S8P–S). This feature is identical to direct transplantation of freshly isolated suture cells undergoing intramembranous ossification (5). In contrast, transplantation of cells from the tibia/femur formed endochondral bones with large marrow cavities (5). The results strongly indicated

that the newly developed culture system can preserve SuSC stemness and properties, permitting their analyses in an ex vivo setting.

Ex vivo characterization of SuSCs

Previous in vivo examinations of mouse SuSCs indicated their quiescence, suggesting their inclusion in the label-retaining cell population (5). To test if SuSC quiescence is also preserved in the ex vivo culture, we performed pulse-chase labeling analyses. Using the *Axin2*$^{Dox\text{-}GFP}$ (genotype: *Axin2-rtTA; TRE-H2BGFP*) mouse model, Axin2-expressing cells were pulse-labeled in vivo with inducible expression of H2BGFP upon 3-day Dox administration (P7-P10) (5). Suture cells were then isolated from these mice at P10, followed by chasing analysis in the absence of Dox for sphere formation. GFP analysis of 1^0 spheres revealed only a single cell with strong fluorescent intensity (Fig. 6A). Similar results were obtained in the subsequent 2^0 and 3^0 cultures (Fig. 6B–C). Although 32% of the 1^0 spheres didn't contain any GFP positive cells, all spheres found in the 2^0 and 3^0 passages are GFP positive (Fig. 6D). This is likely due to the presence of skeletal precursors with limited proliferation ability in the 1^0 culture. These progenitors could form 1^0 spheres but were unable to generate spheres in the subsequent passages. Whole-mount immunostaining of these spheres further indicated this GFP+ label-retaining cell expressing Axin2 (Fig. 6F) but not actively proliferating (Fig. 6G). These results support our hypothesis that SuSCs undergo asymmetric division in which one daughter cell remains undifferentiated, thus showing label-retaining ability (Fig. 6E). The sphere is formed by a single Axin2+ cell undergoing asymmetric division to generate a daughter stem cell and a daughter progenitor. The daughter stem cell becomes quiescent and does not divide again while the rest of the sphere cells with reduced fluorescent intensity are derived from the daughter progenitor with multiple rounds of cell division.

The requirement of Bmpr1a for self-renewal and bone formation of SuSCs

Using ex vivo pulse-chase labeling analysis, we first examined the expression of Bmpr1a in the Axin2-expressing SuSC. Whole-mount immunostaining of the cultured spheres indicated that Bmpr1a is expressed in the GFP+ label-retaining cell expressing Axin2 (Fig. 6H). Bmpr1a is also expressed in a few neighboring cells consistent with our in vivo double-labeling analysis showing a wider expression pattern of Bmpr1a (Fig. S2C–E). Next, we examined the necessity of Bmpr1a for SuSC self-renewal using serial culture analysis. The culture of cells isolated from the P5 control and *Bmpr1a*^{Ax2} sutures showed comparable sphere formation in 1^0 cultures (Fig. 6I). However, the number of 2^0 and 3^0 spheres was significantly reduced in subsequent mutant cultures, suggesting that the self-renewing ability of SuSCs is compromised by the loss of Bmpr1a (Fig. 6I, p-value < 0.05, n=3, mean ± SEM, student t-test). The size of the mutant spheres was also smaller compared to the control (Fig. 6J). Bmpr1a thus plays an essential role in SuSC self-renewal and stemness maintenance in sphere culture. Our prior study showed that SuSC self-renewal is causally linked to clonal expansion and bone regeneration in vivo, especially when a small number of cells are used for transplantation analysis (5). To test if clonal expansion and osteogenic abilities are affected in Bmpr1a-deficient SuSCs, we implanted 30 spheres into the kidney capsule. In this assay, we used 1^0 spheres due to the impaired formation of the mutant spheres in subsequent passages. Ectopic bone formation mediated by *Bmpr1a*^{Ax2} 1^0 suture

spheres was severely impaired (Fig. 6K–N). Only on a rare occasion, we detected a tiny von Kossa stained area in the mutant implant.

To determine the role of Bmpr1a in SuSC-mediated bone formation, we combined sphere culture and kidney capsule transplantation analyses. Using *Bmpr1aFx/Fx* primary cells with infection of lentivirus expressing GFP (control) or Cre, we excluded potential non-cell-autonomous effects of SuSCs that may occur before their isolation in the $Bmpr1a^{Ax2}$ model. The isolated cells, infected by lentivirus-GFP or lentivirus-Cre, were cultured to form spheres, followed by kidney capsule transplantation analysis. The efficiency of lentivirus-mediated expression with minimal toxicity was first determined by the use of lentivirus expressing RFP. At MOI 1, the expression seems optimal without notable alterations of the sphere size and number (Fig. S9A–C). The Cre-dependent deletion of Bmpr1a in suture spheres is highly efficient and drastically reduced the size of the generated bones (Fig. S9D–G; p-value < 0.05, n=3, mean ± SEM, student t-test). These results suggested Bmpr1a essential for clonal expansion (Fig. 6) and bone formation of SuSCs in a cell autonomous manner (Fig. 6 and Fig. S9). Bmpr1a regulates not only SuSC self-renewal but also SuSC-mediated skeletogenesis.

Characterization of human SuSCs

To test the existence of human SuSCs and their isolation, we obtained discards containing unfused sutures from craniosynostosis patients undergoing surgical operations. First, immunostaining identified cells expressing AXIN2 and BMPR1A in the midline of human sutures (Fig. 7A–C and Fig. S10). Then, the isolated human suture cells could grow into 1^0 spheres in single-cell suspension culture with very low seeding density (Fig. 7D). We obtained 2^0 and 3^0 spheres without notable decreases in number and size after serial re-plating (10^4 cells for 1^0-3^0), indicating the presence of human SuSCs with the self-renewing ability (Fig. 7E, F). Whole-mount co-immunostaining further showed the human suture sphere also containing a single Axin2+ cell not actively proliferating (Fig. 7G–I) although some human sphere does not contain Axin2+ cells. In agreement with the animal study, these results indicated that human SuSCs are quiescent and maintain their stemness/identity via asymmetric division. Finally, implantation of human cells into mouse kidney capsules revealed the formation of ectopic bones positive for von Kossa staining in whole-mounts and sections (Fig. 7J–K, 80% success rate, n = 5). Our finding demonstrated successful isolation and culture of human SuSCs, a major hurdle to overcome for translational study.

Bone formation from mouse and human Bmpr1a-expressing cells

The important role of Bmpr1a in stem cell regulation prompted us to test its use as a cell surface marker for SuSC isolation. This is highly possible because Bmpr1a-expressing cells overlap with Axin2-expressing cells in the suture (Fig. S1). Using a specific antibody with fluorescence-activated cell sorting (FACS), we purified Bmpr1a/$BMPR1A^{High}$ and Bmpr1a/$BMPR1A^{Low}$ cell populations from mouse/human sutures (Fig. 8A, G and Fig. S11). Successful bone formation was evident in the animal recipients with implantation of Bmpr1a/$BMPR1A^{High}$ but not Bmpr1a/$BMPR1A^{Low}$ mouse and human suture cells (Fig. 8B–C, H–I). Immunostaining of Osterix identified osteoprogenitor cells surrounding the mineralized tissues generated by transplantation of both mouse Bmpr1a^{High} (Fig. 8D–F)

and human BMPR1A^{High} (Fig. 8J–M) suture cells. The results strongly suggest the use of Bmpr1a/BMPR1A as a SuSC marker. Not only Bmpr1a functionally regulates stem cell stemness essential for suture patency and craniosynostosis but also SuSCs are included in the Bmpr1a/BMPR1A^{High} cell population.

Discussion

This study provides compelling evidence that Bmpr1a is essential for SuSC regulation. The loss of Bmpr1a in Axin2-expressing cells impairs SuSC self-renewal, clonal expansion, and osteogenic abilities. Bmpr1a is required for maintaining these pertinent functions associated with stem cell stemness, implying its role in repressing differentiation. The suppressive effect of BMP signaling on early osteogenesis is also supported by prior reports showing that neonatal disruption of Bmpr1a or its ablation in osteoprogenitor cells increases the osteoblast cell number (31–33). The loss of Bmpr1a reduces Smad phosphorylation and activates P38 and ERK kinases, indicating the balance of canonical and noncanonical BMP signaling cascades is altered in SuSCs. It has been proposed that Bmpr1a regulates this balance through modulation of Tak1 (34). As Tak1 is not activated in the *Bmpr1a*^{Ax2} mutant, our findings suggest a noncanonical pathway distinct from Tak1/MAPK responsible for Bmpr1a-mediated SuSC stemness. In the kidney capsule transplantation, only suture cells positive but not negative for Axin2 can generate bones (5). This implies that skeletal stem cells included in the Axin2 positive cell population have the potent bone-forming ability in the kidney capsule. There are certainly osteogenic precursors and/or osteoblast cells within the Axin2 negative cell population but unable to form ectopic bones. This intriguing observation indicates that osteoblasts, albeit bone-forming cells, are ineffective for bone formation upon transplantation. These results may explain why direct engraftment and replacement for the damaged tissue are difficult to achieve in most cell-based therapies. For their success, the survival, engraftment, and expansion of the transplanted cells seem to be highly critical factors. Only stem cells possess these properties which are preserved by Bmpr1a. The removal of Bmpr1a in the cultured sphere disrupts the bone-forming ability of SuSCs strongly supporting this conclusion. Further elucidation of the regulatory mechanism underlying cell survival and engraftment promises important insight into Bmpr1a-mediated bone regeneration, leading to a new strategy for stem cell-based therapy.

SuSC-specific ablation of Bmpr1a results in precocious differentiation and suture fusion. Our findings reveal a new etiology for craniosynostosis – stem cell depletion. This pathogenetic mechanism is distinct from any established ones, e.g. cell proliferation, differentiation, and apoptosis, known to cause excessive intramembranous ossification (14). It is also different from our previous report in which suture fusion can be caused by stem cell fate switching. SuSCs undergo chondrogenesis instead of osteoblastogenesis, leading to craniosynostosis mediated by ectopic endochondral ossification (18). Stem cell depletion is usually associated with ossification deficiency that may be related to reported patients such as Cole-Carpenter syndrome exhibiting wide-open midline sutures containing intra-sutural bones (35). The intra-sutural bone also known as Wormian bone occurring frequently in disorders with reduced cranial ossification has been associated with craniosynostosis (36). The stem cell depletion mechanism may be explored in synostosis patients without the typically enhanced ossification phenotype.

Although skeletal stem cells residing in the suture were identified recently, their role in craniosynostosis remained unknown (5, 6). Axin2 and Gli1 have been used to identify the skeletal stem cells in the calvarium (5, 6) but the deletion of Bmpr1a in Gli1+ cells does not induce craniosynostosis albeit show enhanced osteoblast proliferation and differentiation (37). This discrepancy may be attributed to Axin2 expression in a more restricted label-retaining cell population – suture midline (5, 6). Also, the expression of Bmpr1a co-localizes with Axin2 but not Gli1 (37). Our results show that Axin2+ SuSCs undergo asymmetric division to maintain quiescence. The disruption of Bmpr1a-dependent regulation of SuSC quiescence is likely the trigger for craniosynostosis. As SuSC stemness is maintained by Bmpr1a, its deletion leads to aberrant ossification initiated at the suture midline. Therefore, craniosynostosis arises from skeletal stem cell deficiency.

Preserving stemness in vitro is critical for bone tissue engineering. Although the sphere-forming cells from the bone marrow have been reported, there is a lack of evidence for their in vivo origin and osteogenic ability (38–40). Whether their stemness can be preserved in vitro remains unknown. We have developed an ex vivo protocol to culture SuSCs for an extended period. The cultured SuSCs can generate bones upon implantation to the ectopic site. Furthermore, the SuSC culture provides an outstanding system for further examination of skeletal stem cell characteristics, e.g. label-retaining ability, asymmetric division, cell fate determination, generation of skeletal progenitors, and skeletogenic differentiation. These are extremely important advancements in stem cell-based therapy for bone regeneration and repair.

To move closer to translating our research, we have identified human BMPR1A-expressing SuSCs capable of generating bones. As Axin2 is an intracellular protein, it is essential for identifying a surface marker for stem cell purification. BMP antagonist Gremlin1 can label skeletal stem cells contributing to endochondral ossification even though the functional importance of BMP signaling remains unclear (8). Our results demonstrate that Bmpr1a is not only a key regulator for SuSCs but can also be used for their isolation. BMPR1A is also known as CD292 designated in CD nomenclature (41). Human and mouse suture cells positive for BMPR1A/CD292 possess skeletal stem cell properties for bone formation. The findings provide compelling evidence for the purification of the human SuSC population.

We have successfully maintained SuSC stemness in culture but it’s limited to five passages. The genetically based cell tracing shows SuSC self-renewing ability for more than one year (5), suggesting potential improvement for long-term culture. Increasing stem cell number is another improvement beneficial for translational implications due to limited cell source. Although the transplanted SuSCs generate intramembranous bones highly reminiscent of calvarial bones, no suture-like structure is present in the kidney capsule. It may be attributed to a lack of niche cells unable to generate suture. We speculate the inclusion of SuSC niche cells essential for ectopic suture generation. Our SuSC study promotes future niche cell identification and isolation, leading to the prevention of suture re-synostosis in surgically operated patients or possibly a preventive procedure for premature suture closure as an alternative to surgical operations. Further elucidation of the mechanism underlying SuSC regulation and SuSC-mediated regeneration promise advancements in our knowledge base of congenital deformity and skeletal repair.

Methods

Study design

This study was designed to identify SuSC regulator. Using an unbiased genomic approach, we found BMP signaling potentially involved in SuSC regulation. We generated mouse models to examine all three BMP type I receptors and revealed Bmpr1a essential for SuSC-mediated calvarial morphogenesis. A time-course study examined aberrant suture closure caused by Bmpr1a loss in SuSCs. These developmental analyses revealed a new mechanism of suture fusion where SuSC-specific disruption of Bmpr1a results in craniosynostosis initiated in the suture midline – stem cell niche, followed by ossification toward both osteogenic fronts. To test if stem cell depletion is the cause of precocious differentiation, we examined stemness, self-renewal, quiescence, stem cell frequency, proliferation, clonal expansion, and bone-generating ability of SuSCs using a variety of ex vivo culture and in vivo transplantation assays. A human SuSC population was also identified and charactered in similar experimental settings. As a cell surface marker, we demonstrated the use of Bmpr1a/BMPR1A to isolate mouse and human SuSCs with genuine skeletal stem cell characteristics. For scientific reproducibility, all studies were performed and repeated with proper controls, including wild-type mice, and mice carrying appropriate transgene(s). Mice of both sexes were examined because of skeletogenesis possibly sensitive to hormones. At least three or five independent experiments were performed for each study. Human samples were obtained from non-syndromic synostosis patients with at least five independent samples used for this study. The analysis of samples by μCT was performed by a technician who is blinded to the condition. No randomization, statistical method to predetermining the sample size, and inclusion/exclusion criteria defining criteria for samples were used.

Animals and models

The *Axin2-rtTA*, *TRE-H2BGFP*, *TRE-Cre*, *R26RTomato*, *Bmpr1aFx, Acvr1Fx, Bmpr1b null, SCID* mouse strains, and genotyping methods were reported previously (18, 25, 42–50). To create $Axin2^{GFP}$ strain (18, 51), mice carrying *Axin2-rtTA* and *TRE-H2BGFP* transgenes were obtained and treated with Dox (2 mg/ml plus 50 mg/ml sucrose) for 3 days as described (42, 43, 48). The $Axin2^{Cre\text{-}Dox}$ mouse strain was generated by obtaining mice carrying *Axin2-rtTA* and *TRE-Cre* transgenes. The $Axin2^{Cre\text{-}Dox}$ mice were then crossed with *Bmpr1aFx*, *Acvr1Fx*, and *R26RTomato* mice to obtain $Bmpr1a^{Ax2}$, $Acvr1^{Ax2}$, and $Axin2^{Cre\text{-}Dox}$; *R26RTomato* mouse, respectively. The expression of Cre in the Axin2-expressing cells was then induced by Dox treatment (18, 52). Both male and female mice were used in this study. Care and use of experimental animals described in this work comply with guidelines and policies of the University Committee on Animal Resources at the University of Rochester.

Cell isolation and purification

Primary suture mesenchymal cells containing SuSCs were isolated from mouse calvaria as described (5). Briefly, an approximately 1.5 mm width tissue containing sagittal suture and its adjacent parietal bones were dissected, followed by separation of the parietal bone parts. Next, the suture parts were incubated with 0.2% collagenase in PBS at 37°C for 1.5 hours. The dissociated cells were filtered, and then re-suspended in DMEM media for

transplantation analysis, in DMEM containing 5% FBS for cell sorting, or in ultra-low attachment surface plate with supplemented media, containing 25 μg/ml insulin, 100 μg/ml transferrin, 20 nM progesterone, 30 nM sodium selenite, 60 nM putrescine, 20 ng/ml EGF, 20 ng/ml bFGF, 20 ng/ml B27 supplement, and 1% penicillin-streptomycin, for sphere culture. After 7–10 days, the spheres were dissociated by 0.25% trypsin-EDTA and seeded as the single-cell suspension for the culture of the next passage. For differentiation, the spheres were transferred to 24 well plates with physical surface treatment (662160, Greiner Bio-One, Monroe, NC) for attachment and cultured in differentiation α-MEM medium containing ascorbic acid (50 μg/ml) and 4 mM β-glycerophosphate for 3 weeks. For alcian blue staining, sphere-derived cells were fixed in a solution containing 30% ethanol, 0.4% paraformaldehyde, and 4% acetic acid for 15 min at room temperature, followed by incubation with 0.05% alcian blue staining solution in 75% ethanol: 0.1M hydrochloride (4:1) overnight at 37°C. For alkaline phosphatase staining, samples were fixed in neutral 10% buffered formalin for 15 min at room temperature, followed by the staining with 1-Step NBT/BCIP Substrate Solution (34042, Thermo Fisher Scientific). For human suture cell isolation, we obtained calvarial discards containing unfused suture of nonsyndromic craniosynostosis patients (3 to 14 months), followed by removal of the bone fragments to obtain the suture mesenchyme and incubation with 0.2% collagenase in PBS for 1.5h at 37°C. The dissociated cells were then filtered through a 40 μm strainer, followed by resuspension in DMEM media containing 20% FBS for sphere culture, or in PBS containing 3% FBS for cell purification. To purify Bmpr1a positive and Bmpr1a negative cell populations, freshly isolated suture cells were stained with primary mouse monoclonal Bmpr1a antibody (MA5–17036, Thermo Fisher Scientific, Waltham, MA), followed by sorting according to the intensity of secondary antibody conjugated Texas Red using FACSAria-II (BD Biosciences, San Jose, CA). The specificity of this Bmpr1a antibody for the isolation of cells expressing high amounts of Bmpr1a was determined by FACS analysis (Fig. S11). The transplantation of freshly isolated cells or cultured sphere cells into the kidney capsule was performed as described (5).

Staining and analysis

Skull preparation, fixation, and embedding for paraffin and frozen sections were performed as described (16, 18, 52, 53). Samples were subject to hematoxylin/eosin staining for histology, Goldner's Trichrome staining, GFP analysis, β-gal staining, van Kossa staining, or immunological staining with avidin:biotinylated enzyme complex (16, 18, 42, 43, 53–57). For antigen retrieval, samples were incubated with antigen unmasking solution (H3300, Vector) in pressured cooking for 10 min or 20 mM Tris-HCl (pH 9) for 16 hr at 70 °C. For *in vitro* deletion of Bmpr1a, cells isolated from mouse *Bmpr1aFx/Fx* suture were infected by Lenti-GFP or Lenti-Cre viruses (MOI = 1). The whole-mount von Kossa staining, immunological staining, in situ hybridization, and double labeling analyses were performed as described (5, 53, 58). For double labeling of von Kossa staining and immunostaining, samples were fixed with 2% paraformaldehyde and 0.02% NP-40 for 1 hour at room temperature, followed by incubation with 1% silver nitrate under ultraviolet light for 30 min, and with 5% sodium thiosulfate for 5min. Then, the stained samples were processed for paraffin sections and subsequent immunological staining. To detect proliferating cells, EdU was added to the sphere for 16 hours after four-day culture, followed by attachment

using Cytospin (Thermo Fisher Scientific). After fixing with 95% ethanol for 5 min on ice and 2% paraformaldehyde for 20 min at room temperature, the spheres were treated with 0.5% Triton-X100 for 10 min and incubated with EdU reaction buffer for 30 min according to the manufacturer's protocol (Thermo Fisher Scientific). Rabbit polyclonal antibodies Osterix (ab22552, Abcam, Cambridge, MA; 1:200), Bmpr1a (ABP-PAB-10536, Allele, San Diego, CA; 1:100), phospho-Tak1 (arb191688, Biorbyt, St Louis, MO; 1:200), phospho-ERK1/2 (4370, Cell Signaling Technology, 1:50); rabbit monoclonal antibodies Ki67 (RM-9106, Thermo Fisher Scientific; 1:200), Axin2 (2151, Cell Signaling Technology; 1:500), phospho-p38 MAPK (4511, Cell Signaling Technology, 1:200), phospho-JNK (4668, Cell Signaling Technology, 1:100) were used for immunostaining. The Bmpr1a antibody (ab264043, Abcam, 1:200) was used for FASC sorting and immunostaining studies. Images were taken using a Zeiss Axio Observer microscope (Carl Zeiss, Thornwood, NY) or Leica DM2500 microscope with a DFC7000T digital imaging system (Leica Biosystems Inc., Buffalo Grove, IL).

Statistics

R software version 3.2.1 or Microsoft Excel 2010 was used for statistical analysis. The significance was determined by two-sided student's t-tests. A p-value of less than 0.05 was considered statistically significant. Before performing the t-tests, the normality of the data distribution was first validated by the Shapiro-Wilk normality test. The activity of signaling pathways in SuSCs was estimated by the active Z score using IPA software (Ingenuity® Systems). Statistical data were presented as mean ± SEM or SD. The stem cell frequency was examined by Extreme Limiting Dilution Analysis (ELDA) software (http://bioinf.wehi.edu.au/software/elda/) with validation of the likelihood ratio test for a single-hit model (59).

Supplementary Material

Refer to Web version on PubMed Central for supplementary material.

Acknowledgments

We thank Yuji Mishina, Karen Lyons, and Vesa Kaartinen for providing *Bmpr1a*, *Bmpr1b*, and *Acvr1* modified mouse strains, respectively, and Justin Lopes, John Martinez, Cynthia Tang, Flow Cytometry Core, and Biomechanics & Multimodal Tissue Imaging Core for assistance. Funding: This work is supported by the National Institutes of Health (DE15654, DE269369) and NYSTEM (C029558) to W.H. Competing interests: Authors declare no competing financial interests. Data and materials availability: *Bmpr1aFx* mouse strain is covered by a materials transfer agreement. Microarray data from three biological replicates of Axin2+ and Axin2− suture cells are available in Gene Expression Omnibus (GSE74849: https://www.ncbi.nlm.nih.gov/geo/).

References

1. Mauffrey C, Barlow BT, Smith W, Management of segmental bone defects. J Am Acad Orthop Surg 23, 143–153 (2015). [PubMed: 25716002]
2. Hernigou P, Poignard A, Beaujean F, Rouard H, Percutaneous autologous bone-marrow grafting for nonunions. Influence of the number and concentration of progenitor cells. J Bone Joint Surg Am 87, 1430–1437 (2005). [PubMed: 15995108]
3. Lo DD, Montoro DT, Grova M, Hyun JS, Chung MT, Wan DC, Longaker MT, Stem Cell-Based Bioengineering of Craniofacial Bone. 379–394 (2013).

4. Panetta NJ, Gupta DM, Longaker MT, Bone regeneration and repair. Curr Stem Cell Res Ther 5, 122–128 (2010). [PubMed: 19941457]
5. Maruyama T, Jeong J, Sheu TJ, Hsu W, Stem cells of the suture mesenchyme in craniofacial bone development, repair and regeneration. Nature communications 7, 10526 (2016).
6. Zhao H, Feng J, Ho TV, Grimes W, Urata M, Chai Y, The suture provides a niche for mesenchymal stem cells of craniofacial bones. Nature cell biology 17, 386–396 (2015). [PubMed: 25799059]
7. Chan CK, Seo EY, Chen JY, Lo D, McArdle A, Sinha R, Tevlin R, Seita J, Vincent-Tompkins J, Wearda T, Lu WJ, Senarath-Yapa K, Chung MT, Marecic O, Tran M, Yan KS, Upton R, Walmsley GG, Lee AS, Sahoo D, Kuo CJ, Weissman IL, Longaker MT, Identification and specification of the mouse skeletal stem cell. Cell 160, 285–298 (2015). [PubMed: 25594184]
8. Worthley DL, Churchill M, Compton JT, Tailor Y, Rao M, Si Y, Levin D, Schwartz MG, Uygur A, Hayakawa Y, Gross S, Renz BW, Setlik W, Martinez AN, Chen X, Nizami S, Lee HG, Kang HP, Caldwell JM, Asfaha S, Westphalen CB, Graham T, Jin G, Nagar K, Wang H, Kheirbek MA, Kolhe A, Carpenter J, Glaire M, Nair A, Renders S, Manieri N, Muthupalani S, Fox JG, Reichert M, Giraud AS, Schwabe RF, Pradere JP, Walton K, Prakash A, Gumucio D, Rustgi AK, Stappenbeck TS, Friedman RA, Gershon MD, Sims P, Grikscheit T, Lee FY, Karsenty G, Mukherjee S, Wang TC, Gremlin 1 identifies a skeletal stem cell with bone, cartilage, and reticular stromal potential. Cell 160, 269–284 (2015). [PubMed: 25594183]
9. Newton PT, Li L, Zhou B, Schweingruber C, Hovorakova M, Xie M, Sun X, Sandhow L, Artemov AV, Ivashkin E, Suter S, Dyachuk V, El Shahawy M, Gritli-Linde A, Bouderlique T, Petersen J, Mollbrink A, Lundeberg J, Enikolopov G, Qian H, Fried K, Kasper M, Hedlund E, Adameyko I, Savendahl L, Chagin AS, A radical switch in clonality reveals a stem cell niche in the epiphyseal growth plate. Nature 567, 234–238 (2019). [PubMed: 30814736]
10. Mizuhashi K, Ono W, Matsushita Y, Sakagami N, Takahashi A, Saunders TL, Nagasawa T, Kronenberg HM, Ono N, Resting zone of the growth plate houses a unique class of skeletal stem cells. Nature 563, 254–258 (2018). [PubMed: 30401834]
11. Zhou BO, Yue R, Murphy MM, Peyer JG, Morrison SJ, Leptin-receptor-expressing mesenchymal stromal cells represent the main source of bone formed by adult bone marrow. Cell Stem Cell 15, 154–168 (2014). [PubMed: 24953181]
12. Ornitz DM, Marie PJ, Fibroblast growth factor signaling in skeletal development and disease. Genes & development 29, 1463–1486 (2015). [PubMed: 26220993]
13. Chan CK, Chen CC, Luppen CA, Kim JB, DeBoer AT, Wei K, Helms JA, Kuo CJ, Kraft DL, Weissman IL, Endochondral ossification is required for haematopoietic stem-cell niche formation. Nature 457, 490–494 (2009). [PubMed: 19078959]
14. Opperman LA, Cranial sutures as intramembranous bone growth sites. Dev Dyn 219, 472–485 (2000). [PubMed: 11084647]
15. Wilkie AO, Morriss-Kay GM, Genetics of craniofacial development and malformation. Nature reviews. Genetics 2, 458–468 (2001).
16. Yu HM, Jerchow B, Sheu TJ, Liu B, Costantini F, Puzas JE, Birchmeier W, Hsu W, The role of Axin2 in calvarial morphogenesis and craniosynostosis. Development (Cambridge, England) 132, 1995–2005 (2005).
17. Yilmaz E, Mihci E, Guzel Nur B, Alper OM, A novel AXIN2 gene mutation in sagittal synostosis. Am J Med Genet A 176, 1976–1980 (2018). [PubMed: 30088857]
18. Maruyama T, Mirando AJ, Deng CX, Hsu W, The balance of WNT and FGF signaling influences mesenchymal stem cell fate during skeletal development. Sci Signal 3, ra40 (2010). [PubMed: 20501936]
19. Kramer A, Green J, Pollard J Jr., Tugendreich S, Causal analysis approaches in Ingenuity Pathway Analysis. Bioinformatics 30, 523–530 (2014). [PubMed: 24336805]
20. Li X, Cao X, BMP signaling and skeletogenesis. Ann N Y Acad Sci 1068, 26–40 (2006). [PubMed: 16831903]
21. Massague J, TGF-beta signal transduction. Annu Rev Biochem 67, 753–791 (1998). [PubMed: 9759503]

22. Mishina Y, Suzuki A, Ueno N, Behringer RR, Bmpr encodes a type I bone morphogenetic protein receptor that is essential for gastrulation during mouse embryogenesis. Genes & development 9, 3027–3037 (1995). [PubMed: 8543149]

23. Gu Z, Reynolds EM, Song J, Lei H, Feijen A, Yu L, He W, MacLaughlin DT, van J Raaij den Eijnden-van, Donahoe PK, Li E, The type I serine/threonine kinase receptor ActRIA (ALK2) is required for gastrulation of the mouse embryo. Development (Cambridge, England) 126, 2551–2561 (1999).

24. Mishina Y, Crombie R, Bradley A, Behringer RR, Multiple roles for activin-like kinase-2 signaling during mouse embryogenesis. Developmental biology 213, 314–326 (1999). [PubMed: 10479450]

25. Yi SE, Daluiski A, Pederson R, Rosen V, Lyons KM, The type I BMP receptor BMPRIB is required for chondrogenesis in the mouse limb. Development (Cambridge, England) 127, 621–630 (2000).

26. Williams H, Lumps, bumps and funny shaped heads. Arch Dis Child Educ Pract Ed 93, 120–128 (2008). [PubMed: 18644899]

27. Rahman MS, Akhtar N, Jamil HM, Banik RS, Asaduzzaman SM, TGF-beta/BMP signaling and other molecular events: regulation of osteoblastogenesis and bone formation. Bone Res 3, 15005 (2015). [PubMed: 26273537]

28. Greenblatt MB, Shim JH, Zou W, Sitara D, Schweitzer M, Hu D, Lotinun S, Sano Y, Baron R, Park JM, Arthur S, Xie M, Schneider MD, Zhai B, Gygi S, Davis R, Glimcher LH, The p38 MAPK pathway is essential for skeletogenesis and bone homeostasis in mice. J Clin Invest 120, 2457–2473 (2010). [PubMed: 20551513]

29. Wang Y, Sun M, Uhlhorn VL, Zhou X, Peter I, Martinez-Abadias N, Hill CA, Percival CJ, Richtsmeier JT, Huso DL, Jabs EW, Activation of p38 MAPK pathway in the skull abnormalities of Apert syndrome Fgfr2(+P253R) mice. BMC Dev Biol 10, 22 (2010). [PubMed: 20175913]

30. Shukla V, Coumoul X, Wang RH, Kim HS, Deng CX, RNA interference and inhibition of MEK-ERK signaling prevent abnormal skeletal phenotypes in a mouse model of craniosynostosis. Nature genetics 39, 1145–1150 (2007). [PubMed: 17694057]

31. Lim J, Shi Y, Karner CM, Lee SY, Lee WC, He G, Long F, Dual function of Bmpr1a signaling in restricting preosteoblast proliferation and stimulating osteoblast activity in mouse. Development (Cambridge, England) 143, 339–347 (2016).

32. Zhang J, Niu C, Ye L, Huang H, He X, Tong WG, Ross J, Haug J, Johnson T, Feng JQ, Harris S, Wiedemann LM, Mishina Y, Li L, Identification of the haematopoietic stem cell niche and control of the niche size. Nature 425, 836–841 (2003). [PubMed: 14574412]

33. Kamiya N, Ye L, Kobayashi T, Mochida Y, Yamauchi M, Kronenberg HM, Feng JQ, Mishina Y, BMP signaling negatively regulates bone mass through sclerostin by inhibiting the canonical Wnt pathway. Development (Cambridge, England) 135, 3801–3811 (2008).

34. Kua HY, Liu H, Leong WF, Li L, Jia D, Ma G, Hu Y, Wang X, Chau JF, Chen YG, Mishina Y, Boast S, Yeh J, Xia L, Chen GQ, He L, Goff SP, Li B, c-Abl promotes osteoblast expansion by differentially regulating canonical and non-canonical BMP pathways and p16INK4a expression. Nature cell biology 14, 727–737 (2012). [PubMed: 22729085]

35. Amor DJ, Savarirayan R, Schneider AS, Bankier A, New case of Cole-Carpenter syndrome. American journal of medical genetics 92, 273–277 (2000). [PubMed: 10842295]

36. Sanchez-Lara PA, Graham JM Jr., Hing AV, Lee J, Cunningham M, The morphogenesis of wormian bones: a study of craniosynostosis and purposeful cranial deformation. Am J Med Genet A 143A, 3243–3251 (2007). [PubMed: 18000970]

37. Guo Y, Yuan Y, Wu L, Ho TV, Jing J, Sugii H, Li J, Han X, Feng J, Guo C, Chai Y, BMP-IHH-mediated interplay between mesenchymal stem cells and osteoclasts supports calvarial bone homeostasis and repair. Bone Res 6, 30 (2018). [PubMed: 30345151]

38. Isern J, Martin-Antonio B, Ghazanfari R, Martin AM, Lopez JA, del Toro R, Sanchez-Aguilera A, Arranz L, Martin-Perez D, Suarez-Lledo M, Marin P, Van Pel M, Fibbe WE, Vazquez J, Scheding S, Urbano-Ispizua A, Mendez-Ferrer S, Self-renewing human bone marrow mesenspheres promote hematopoietic stem cell expansion. Cell reports 3, 1714–1724 (2013). [PubMed: 23623496]

39. Shiota M, Heike T, Haruyama M, Baba S, Tsuchiya A, Fujino H, Kobayashi H, Kato T, Umeda K, Yoshimoto M, Nakahata T, Isolation and characterization of bone marrow-derived mesenchymal

progenitor cells with myogenic and neuronal properties. Experimental cell research 313, 1008–1023 (2007). [PubMed: 17289022]

40. Debnath S, Yallowitz AR, McCormick J, Lalani S, Zhang T, Xu R, Li N, Liu Y, Yang YS, Eiseman M, Shim JH, Hameed M, Healey JH, Bostrom MP, Landau DA, Greenblatt MB, Discovery of a periosteal stem cell mediating intramembranous bone formation. Nature 562, 133–139 (2018). [PubMed: 30250253]
41. Engel P, Boumsell L, Balderas R, Bensussan A, Gattei V, Horejsi V, Jin BQ, Malavasi F, Mortari F, Schwartz-Albiez R, Stockinger H, van Zelm MC, Zola H, Clark G, CD Nomenclature 2015: Human Leukocyte Differentiation Antigen Workshops as a Driving Force in Immunology. J Immunol 195, 4555–4563 (2015). [PubMed: 26546687]
42. Yu HM, Liu B, Costantini F, Hsu W, Impaired neural development caused by inducible expression of Axin in transgenic mice. Mechanisms of development 124, 146–156 (2007). [PubMed: 17123792]
43. Yu HM, Liu B, Chiu SY, Costantini F, Hsu W, Development of a unique system for spatiotemporal and lineage-specific gene expression in mice. Proceedings of the National Academy of Sciences of the United States of America 102, 8615–8620 (2005). [PubMed: 15941831]
44. Mishina Y, Hanks MC, Miura S, Tallquist MD, Behringer RR, Generation of Bmpr/Alk3 conditional knockout mice. Genesis 32, 69–72 (2002). [PubMed: 11857780]
45. Dudas M, Sridurongrit S, Nagy A, Okazaki K, Kaartinen V, Craniofacial defects in mice lacking BMP type I receptor Alk2 in neural crest cells. Mechanisms of development 121, 173–182 (2004). [PubMed: 15037318]
46. Madisen L, Zwingman TA, Sunkin SM, Oh SW, Zariwala HA, Gu H, Ng LL, Palmiter RD, Hawrylycz MJ, Jones AR, Lein ES, Zeng H, A robust and high-throughput Cre reporting and characterization system for the whole mouse brain. Nature neuroscience 13, 133–140 (2010). [PubMed: 20023653]
47. Tumbar T, Guasch G, Greco V, Blanpain C, Lowry WE, Rendl M, Fuchs E, Defining the epithelial stem cell niche in skin. Science (New York, N.Y 303, 359–363 (2004).
48. Hsu W, Mirando AJ, Yu HM, Manipulating gene activity in Wnt1-expressing precursors of neural epithelial and neural crest cells. Dev Dyn 239, 338–345 (2010). [PubMed: 19653308]
49. Maruyama EO, Yu HM, Jiang M, Fu J, Hsu W, Gpr177 deficiency impairs mammary development and prohibits Wnt-induced tumorigenesis. PLoS ONE 8, e56644 (2013). [PubMed: 23457599]
50. Snippert HJ, van der Flier LG, Sato T, van Es JH, van den Born M, Kroon-Veenboer C, Barker N, Klein AM, van Rheenen J, Simons BD, Clevers H, Intestinal crypt homeostasis results from neutral competition between symmetrically dividing Lgr5 stem cells. Cell 143, 134–144 (2010). [PubMed: 20887898]
51. Fu J, Jiang M, Mirando AJ, Yu HM, Hsu W, Reciprocal regulation of Wnt and Gpr177/mouse Wntless is required for embryonic axis formation. Proceedings of the National Academy of Sciences of the United States of America 106, 18598–18603 (2009). [PubMed: 19841259]
52. Mirando AJ, Maruyama T, Fu J, Yu HM, Hsu W, Beta-catenin/cyclin D1 mediated development of suture mesenchyme in calvarial morphogenesis. BMC Dev Biol 10, 116 (2010). [PubMed: 21108844]
53. Maruyama T, Jiang M, Hsu W, Gpr177, a novel locus for bone mineral density and osteoporosis, regulates osteogenesis and chondrogenesis in skeletal development. J Bone Miner Res 28, 1150–1159 (2013). [PubMed: 23188710]
54. Chiu SY, Asai N, Costantini F, Hsu W, SUMO-Specific Protease 2 Is Essential for Modulating p53-Mdm2 in Development of Trophoblast Stem Cell Niches and Lineages. PLoS biology 6, e310 (2008). [PubMed: 19090619]
55. Fu J, Hsu W, Epidermal Wnt controls hair follicle induction by orchestrating dynamic signaling crosstalk between the epidermis and dermis. J Invest Dermatol 133, 890–898 (2013). [PubMed: 23190887]
56. Russell HK Jr., A modification of Movat's pentachrome stain. Archives of pathology 94, 187–191 (1972). [PubMed: 4114784]

57. Fu J, Yu HM, Chiu SY, Mirando AJ, Maruyama EO, Cheng JG, Hsu W, Disruption of SUMO-Specific Protease 2 Induces Mitochondria Mediated Neurodegeneration. PLoS genetics 10, e1004579 (2014). [PubMed: 25299344]

58. Maruyama T, Jiang M, Abbott A, Yu HI, Huang Q, Chrzanowska-Wodnicka M, Chen EI, Hsu W, Rap1b is an effector of Axin2 regulating crosstalk of signaling pathways during skeletal development. J Bone Miner Res, (2017).

59. Hu Y, Smyth GK, ELDA: extreme limiting dilution analysis for comparing depleted and enriched populations in stem cell and other assays. J Immunol Methods 347, 70–78 (2009). [PubMed: 19567251]

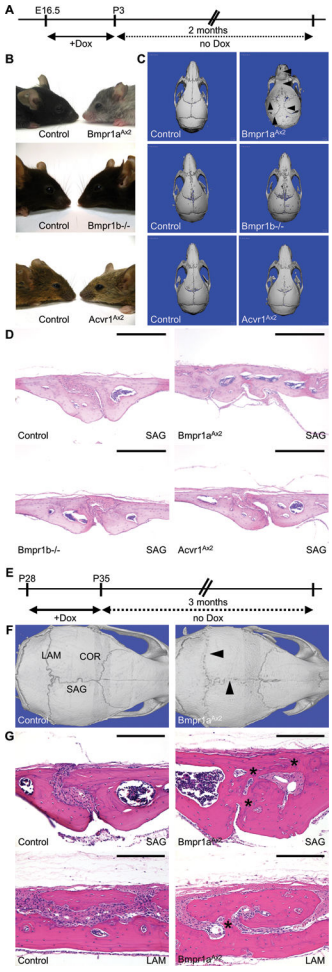

Fig. 1.

Stem cell-mediated calvarial development and homeostasis require Bmpr1a. *Bmpr1a*^{Ax2}, *Bmpr1a−/−* and *Acvr1*^{Ax2} mouse models examine the BMP type I receptor in calvarial morphogenesis. (A) Diagram illustrates the use of the *Axin2*$^{Cre\text{-}Dox}$ (*Axin2-rtTA; TRE-Cre*) system to perform spatiotemporal-specific deletion of Bmpr1a or Acvr1 in Axin2+ SuSCs. In *Bmpr1a*^{Ax2} and *Acvr1*^{Ax2} mice, Dox is administrated from E16.5 to P3 for Cre expression. *Bmpr1b−/−* are homozygous null mice for Bmpr1b. Gross examination (B, E, H), μCT (C-D, F-G, I-J), and hematoxylin and eosin staining (K-N) analyses are then performed at 2 months. Arrowheads indicate *Bmpr1a*^{Ax2} suture abnormality. Note craniosynostosis is only detected in the Bmpr1a mutants. Images are representatives of three independent experiments. (O) Diagram illustrates the deletion of Bmpr1a in adult SuSCs. Dox is administrated from P28 to P35 for Cre expression. Three months later, μCT analysis (P-Q) and hematoxylin and eosin staining (R-U) examine suture closure defects. COR, coronal suture; LAM, lambdoid suture; SAG, sagittal suture. Arrowheads and asterisks indicate aberrant suture closure. Images are representatives of three independent experiments. Scale bars, 400 μm (K-N); 200 μm (R-U).

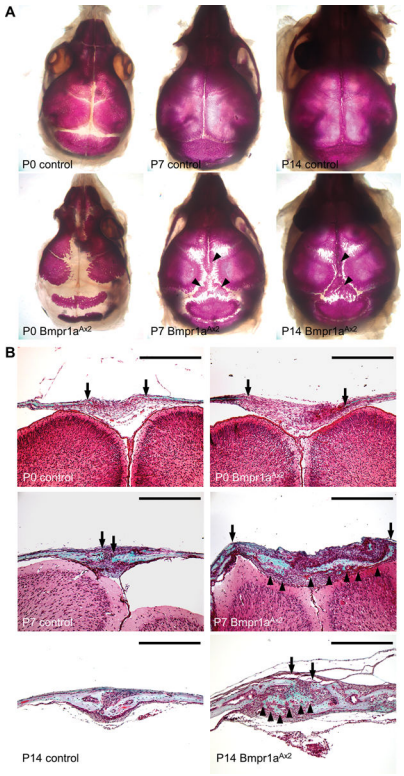

Fig. 2.

Craniosynostosis caused by SuSC-specific disruption of Bmpr1a involves an unusual suture closure process. The control and *Bmpr1a*^{Ax2} calvaria are analyzed by alizarin red (A-F) and Goldner's trichrome (G-L) staining in whole mounts (A-F) and sections (G-L) at P0 (A, D, G-H), P7 (B, E, I-J) and P14 (C, F, K-L). Mineralization arising in the suture midline is evident between calvarial bone plates as indicated by arrowheads. Arrows indicate osteogenic fronts. Images are representatives of three independent experiments. Scale bar, 400 μm (G-L).

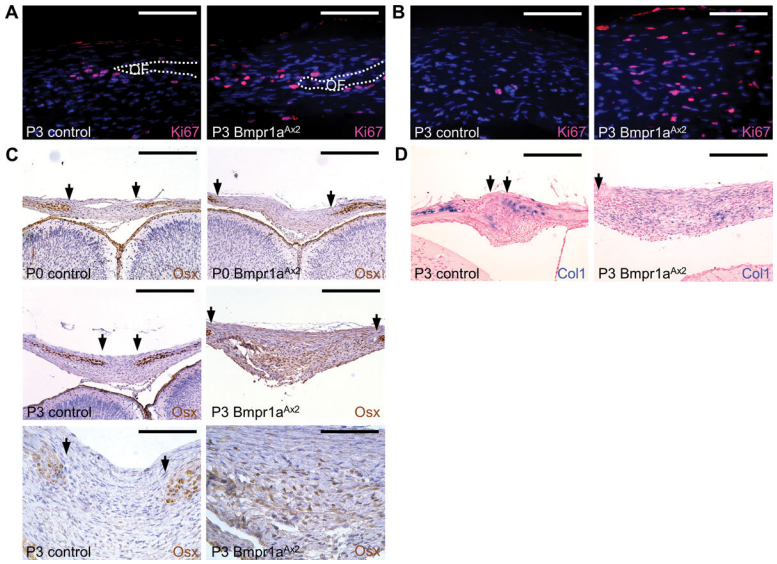

Fig. 3.

The loss of Bmpr1a in SuSCs leads to aberrant intramembranous ossifications within the suture mesenchyme. (A-D) Immunostaining of Ki67 identifies cells undergoing mitotic division in the osteogenic front (A-B; OF) and suture mesenchyme (C-D) of control and *Bmpr1a*^{Ax2} sutures at P3. Sections of the P0 and P3 control and *Bmpr1a*^{Ax2} calvaria are examined by immunostaining of Osterix (Osx; E-J) and in situ hybridization of type1 collagen (Col1; K-L). Arrows indicate osteogenic fronts (OF). Images are representatives of three independent experiments. Scale bars, 60 μm (A-D); 100 μm (I-J); 400 μm (E-H); 200 μm (K-L).

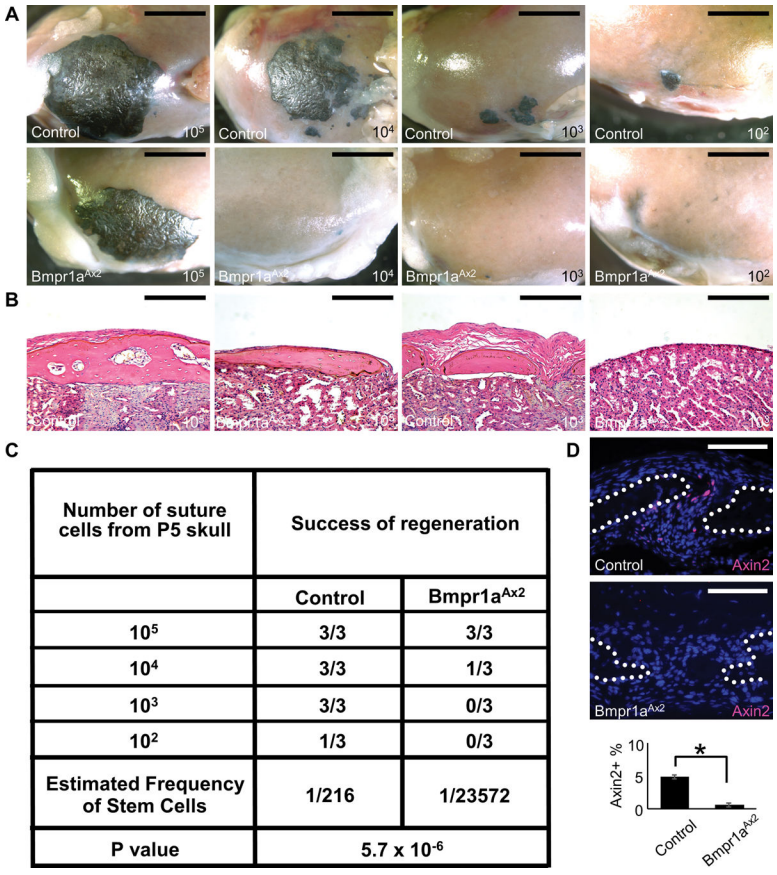

Number of suture cells from P5 skull	Success of regeneration	
	Control	Bmpr1a^{Ax2}
10^5	3/3	3/3
10^4	3/3	1/3
10^3	3/3	0/3
10^2	1/3	0/3
Estimated Frequency of Stem Cells	1/216	1/23572
P value	5.7 x 10^{-6}	

Fig. 4.

Bmpr1a regulates SuSCs and stem cell-dependent bone formation. (A-L) Kidney capsule transplantation with limiting dilution analysis of control and *Bmpr1a*^{Ax2} cells, isolated from the P5 suture mesenchyme with Dox treatment from E16.5 to P3, examines SuSC frequency. Ectopic bone formation is assessed by von Kossa staining in whole mounts (A-H) and histology in sections (I-L). (M) Limiting dilution analysis shows the success of bone formation with transplantation of 10^5, 10^4, 10^3, and 10^2 cells, providing a quantitative estimation for stem cell frequency using ELDA software. (N-O) Sections of the P7 sagittal suture are examined by immunostaining of Axin2 and counterstaining with DAPI. Broken lines define the calvarial bones. (P) The graph shows the average percentage of Axin2-expressing cells in control and mutant sutures (asterisk, $p < 0.01$, n=3, mean ± SEM, student t-test). Note Axin2+ SuSCs is reduced by Bmpr1a deficiency. Images are representatives of three independent experiments. Scale bars, 4mm (A-J); 200 μm (I-L); 100 μm (N-O).

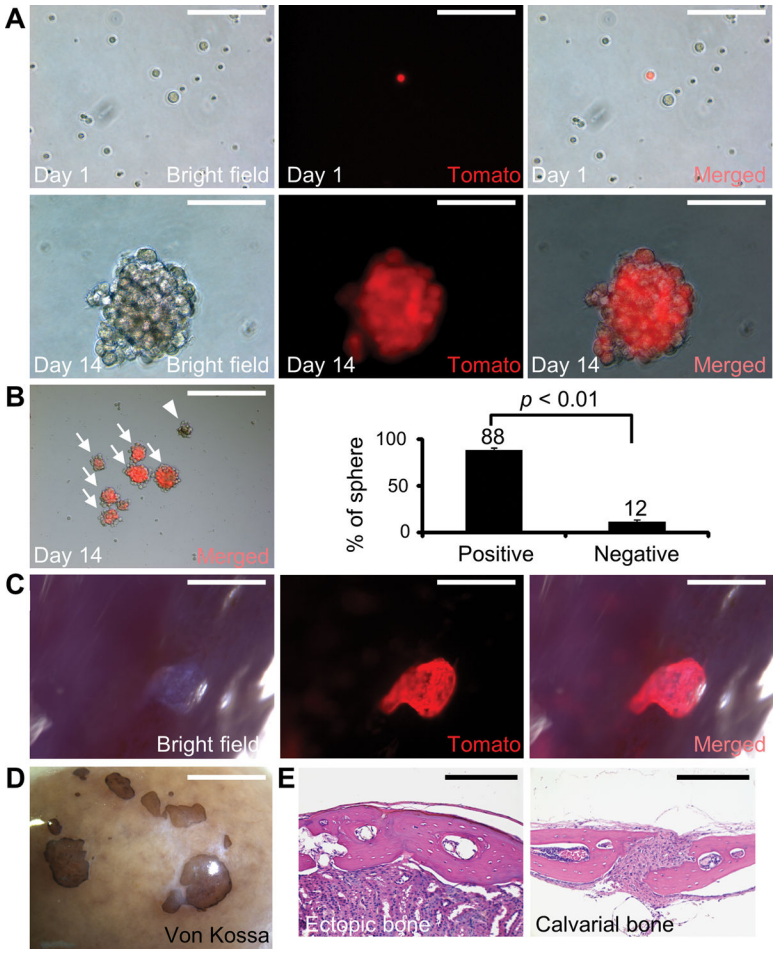

Fig. 5.

SuSC stemness is preserved in sphere culture. (A-G) Genetic cell-labeling traces the fate of Axin2+ SuSCs using the *Axin2*$^{Cre\text{-}Dox}$*; R26RTomato* model. Fluorescent imaging identifies Axin2+ SuSCs before tracing (A-C) and Axin2+ SuSCs and their derivatives after tracing for 14 days in culture (D-G). Arrows and arrowheads indicate the formation of spheres from Axin2+ and Axin2– cells, respectively. (H) Graphs show the average percentage of spheres derived from Axin2 positive and negative cells ($p < 0.01$, n=3, mean ± SEM, student t-test). (I-K) Whole-mount imaging reveals successful colonization and growth of SuSC spheres 4 weeks after transplantation into the kidney capsule. (L) Whole-mount von Kossa staining identifies ectopic bones generated by SuSC spheres 8 weeks after transplantation. Hematoxylin and eosin staining show the generation of ectopic bone (M) resembling calvarial bone plate (N). Images are representatives of three independent experiments. Scale bars, 100 μm (A-F); 400 μm (G); 1 mm (I-K); 2 mm (L); 200 μm (M-N).

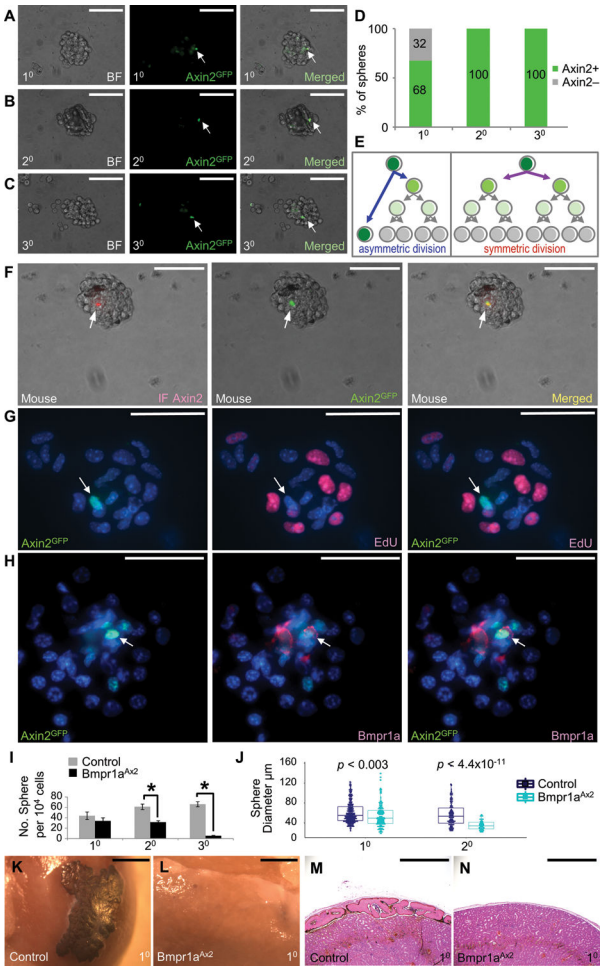

Fig. 6.

Bmpr1a is essential for SuSC self-renewal. (A-C) Ex vivo pulse-chase labeling analysis of cells isolated from *Axin2*^{GFP} mouse sutures examines quiescence of SuSCs in 1^0, 2^0, and 3^0 cultures. Whole-mount imaging reveals a single label-retaining cell with strong GFP intensity in the cultured spheres (arrows). (D) Diagrams show the percent of spheres with (Axin2+) or without (Axin2–) the label-retaining cell and derivatives of Axin2-expressing cells in different passages. (E) Schemes illustrate GFP+ label-retaining cells in the sphere under the asymmetric but not symmetric division of SuSCs. (F-G) Ex vivo pulse-chase labeling followed by whole-mount immunostaining examines label-retaining and Axin2-expressing cells (F), or cells undergoing mitotic division (G), in the suture spheres, respectively. Arrows indicate a single label-retaining cell stained positive for Axin2 (F) but negative for EdU (G). (H) Ex vivo pulse-chase labeling followed by whole-mount immunostaining of Bmpr1a in the suture spheres. Arrows indicate a single label-retaining cell stained positive for Axin2 and Bmpr1a. In vitro self-renewal is examined by serial culturing of spheres. Diagrams illustrate the sphere number (I) and size (J) affected by the loss of Bmpr1a. The suture sphere number is significantly reduced in the 2^0 and 3^0 cultures of *Bmpr1a*^{Ax2} compared to the control (asterisks, $p < 0.05$, n=3, mean ± SEM, student t-test). The average sphere size is also reduced in the mutant cultures (p-value determined by the two-sided student t-test, 1^0 control: 236 spheres, and *Bmpr1a*^{Ax2}: 188 spheres; 2^0

control: 124 spheres, and Bmpr1a^{Ax2}: 66 spheres, n=3). Whole-mount von Kossa staining (K-L) and histological (M-N) analyses of the kidney capsules transplanted with the 1^0 spheres show that the osteogenic ability is maintained in control but impaired in *Bmpr1a*^{Ax2} spheres. Images are representatives of three independent experiments. Scale bars, 100 μm (A-C, F); 50 μm (G-H); 2 mm (K-L); 800 μm (M-N).

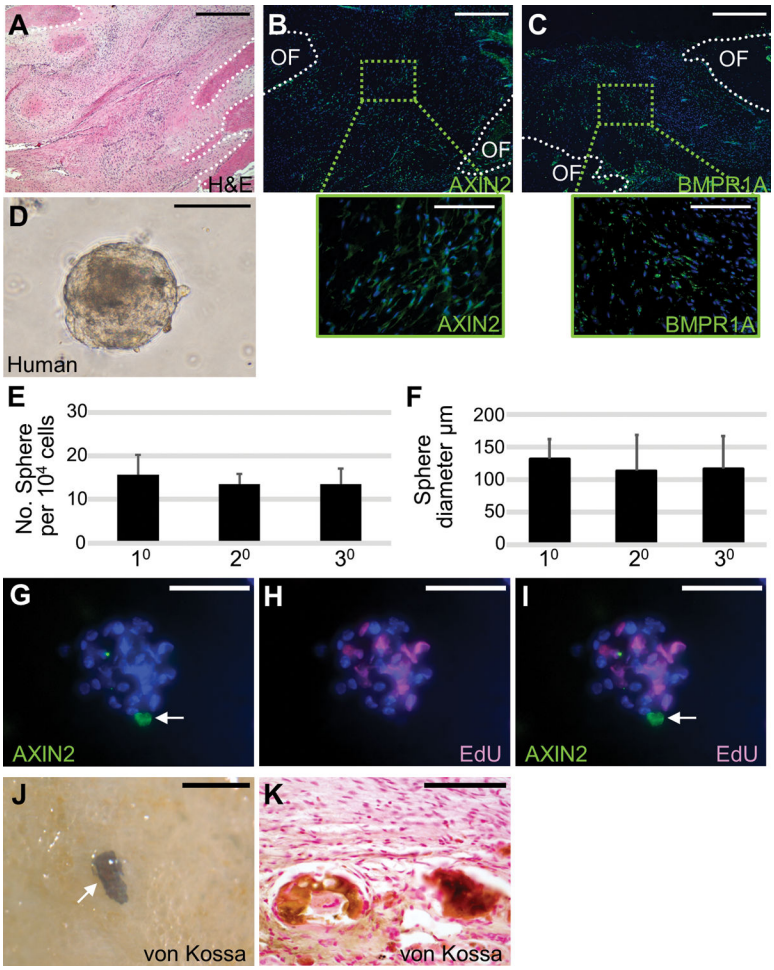

Fig. 7.

Self-renewal and osteogenic ability of human SuSCs. Sections of the 14-month-old human coronal suture were examined by hematoxylin and eosin staining (A), immunostaining of AXIN2 (B), and BMPR1A (C). Broken lines define the calvarial bones at the osteogenic front (OF). (D) Cells isolated from human suture form spheres in ex vivo culture. Diagrams illustrate the average number (E, n=5, mean ± SD) and size (F, n=5, >15 spheres in each passage, mean ± SD) of spheres formed by the 1^0, 2^0, and 3^0 culture of human suture cells starting with 10^4 cells for each passage. (G-I) Co-immunostaining of the human sphere after pulse-chase labeling identifies a single AXIN2-expressing cell (arrow) and EdU positive cells undergoing mitotic division. The von Kossa staining in whole-mounts (J) and sections (K) shows ectopic bone formation in the kidney capsule with implantation of human suture cells. Images are the representatives of at least five independent experiments. Scale bars, 500 µm (A-C); 100 µm (B-C insets, D, G-I, K); 300 µm (J).

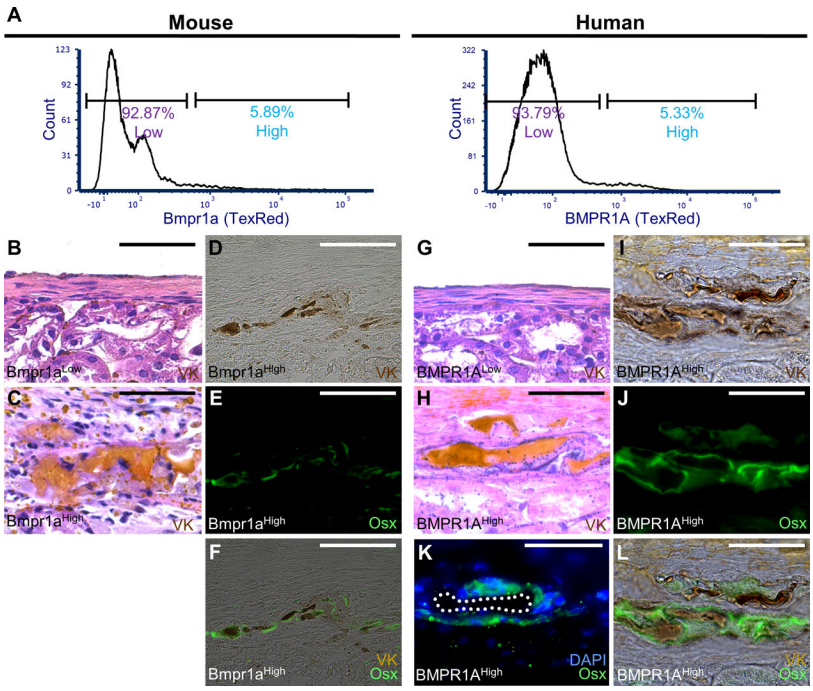

Fig. 8.

The osteogenic ability of mouse and human Bmpr1a-expressing suture cells. Cell sorter purifies Bmpr1a^{High} and Bmpr1a^{Low} cell populations from mouse (A) and human (G) suture mesenchymes, followed by bone formation study in the kidney capsule (B-F, H-M). von Kossa staining of the transplanted kidneys shows bone formation from 5×10^3 Bmpr1a/BMPR1A^{High} (C-F, I-M) but not Bmpr1a/BMPR1A^{Low} (B, H) cells isolated from mouse (B-F) and human (H-M) skulls. Immunostaining of Osx identifies osteoprogenitor cells surrounding the von Kossa stained bone (D-F, J-M). Images are the representatives of at least five independent experiments. Scale bars, 50 μm (B-C, H-M), 100 μm (D-F).